Energy 271 (2023) 126968

Contents lists available at ScienceDirect

Energy

journal homepage: www.elsevier.com/locate/energy

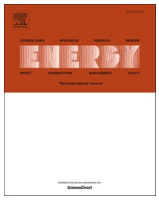

Machine learning prediction of fuel properties of hydrochar from co-hydrothermal carbonization of sewage sludge and lignocellulosic biomass

Oraléou Sangué Djandja [a,b,e], Shimin Kang [a,*], Zizhi Huang [a], Junqiao Li [a], Jiaqi Feng [a], Zaiming Tan [a], Adekunlé Akim Salami [c], Bachirou Guene Lougou [d]

[a] Engineering Research Center of None-food Biomass Efficient Pyrolysis and Utilization Technology of Guangdong Higher Education Institutes, Guangdong Provincial Key Laboratory of Distributed Energy Systems, Dongguan University of Technology, Dongguan, Guangdong, 523808, China
[b] School of Environmental Science and Engineering, Tianjin University, Tianjin, 300350, China
[c] Centre D'Excellence Régional pour La Maîtrise de L'Electricité (CERME), Université de Lomé, Lomé, BP 1515, Togo
[d] School of Energy Science and Engineering, Harbin Institute of Technology, 92 West Dazhi Street, Harbin, 150001, China
[e] Organization of African Academic Doctors (OAAD), Off Kamiti Road, P. O. Box 25305000100, Nairobi, Kenya

ARTICLE INFO

Keywords:
Sewage sludge
Lignocellulosic biomass
Hydrothermal carbonization
Fuel
Machine learning

ABSTRACT

Machine learning approaches are emerging as a promising method for assisting in the control of thermochemical processes. eXtreme Gradient Boosting (XGB) and Random Forest (RF) were applied, for the first time, for prediction of fuel properties of hydrochar from co-hydrothermal carbonization of sewage sludge (SS) and biomass. XGB outperformed RF in the prediction of carbon content, O/C, higher heating value, and mass and energy yields, while RF surpassed XGB in the prediction of H/C, N/C, and fuel ratio. The R^2 between the predicted and experimental values for the best models was in [0.94–1] and [0.83–0.95], respectively for training and test. The feature importance and partial dependence analyses were used to interpret models and provide comprehensive understanding of the input features' impact. Based on the best models, a graphical user interface was created to make prediction easier for other researchers. By only knowing the properties of SS and lignocellulosic biomass, the authors could prior to experiments explore various co-HTC conditions and SS ratios to find the most appropriate conditions to obtain some given properties of hydrochar. This will save time and resources that are usually spent on several trial experiments that may sometimes not yield positive results.

1. Introduction

COP26 meeting in Glasgow urged the consideration of waste and residues in the supply of biofuels and bio-based materials [1]. Therefore, efforts are being initiated towards this goal, and many thermochemical and biochemical processes are being examined for the conversion of various biowastes into valuables biofuels. Among the available processes, hydrothermal carbonization (HTC) has gained popularity for the processing of wet organic waste, mainly sewage sludge (SS) which is a major municipal solid waste that cannot be prevented and is seen as a global critical environmental issue. However, the heterogeneous nature, the relatively lower carbon content and significant nitrogen and ash contents of SS limit the quality of the hydrochar for solid fuel application [2]. Considering this, recent interest has focused on substituting a portion of SS with lignocellulosic biomass during the HTC, and this is named "co-HTC".

Several studies have reported an improved fuel properties of the co-HTC resulting hydrochar when compared to the raw SS, the mixture of SS and the lignocellulosic biomass or the hydrochar from SS alone [3–7]. The improved combustion properties not only relate to the heating release, but also to the potential reduction of ecotoxicity risk. The co-HTC is hence reported as a potential economical and feasible approach to enhance the fuel properties of the hydrochar with reduced environmental impact when combusted [5–7].

Various features of the resulting hydrochar are reported to impact on the fuel properties of the hydrochar when combusted. Higher carbon content leads to improved HHV that defines the amount of the available thermal energy produced by a complete combustion of the hydrochar. Relatively lower atomic ratios of H/C and O/C are reported to improve

* Corresponding author.
E-mail address: kangshimin@dgut.edu.cn (S. Kang).

https://doi.org/10.1016/j.energy.2023.126968
Received 22 September 2022; Received in revised form 19 January 2023; Accepted 14 February 2023
Available online 24 February 2023

List of acronyms and abbreviations

Subscripts

s	Sewage sludge
b	lignocellulosic biomass
h	hydrochar

Abbreviations

ML	Machine Learning
XGB	eXtreme Gradient Boosting
RF	Random Forest
RMSE	Root mean square error
R^2	Square of the correlation coefficient
SHAP	SHapley Additive Explanation
HTC	Hydrothermal carbonization
RT	Reaction temperature
Rt	Reaction time (min)
SSratio	Ratio of sewage sludge in the feedstock mixture (wt.%, db)
SL	Solid loading in the reaction system (wt.%)
SS	Sewage sludge
C	Carbon content (wt.%, db)
H	Hydrogen content (wt.%, db)
N	Nitrogen content (wt.%, db)
O	Oxygen content (wt.%, db)
V	Volatile matter content (wt.%, db)
FC	Fixed carbon content (wt.%, db)
A	Ash content (wt.%, db)
HHV	Higher heating value
MY	Mass yield of the hydrochar
EY	Energy yield of the hydrochar

the fuel properties via the reduction of smoke, water vapor, and energy losses during the combustion of the solid fuel [8,9]. Higher fuel ratio defining an improved stability of the hydrochar, can increase the firing temperature, provide greater flame stability (maintaining less violent flame) and reduce heat loss during combustion [10]. Reduced volatile matter content (resulting in high fuel ratio, and lower H/C and O/C ratios) is also expected to increase the ignition temperature of the hydrochar [3,8], confirming that the hydrochar is safer during handling, storage, and transportation [3]. Lower N/C ratio is good to expect lower NOx emission during combustion. Hence, these features are of great importance for the fuel application of the hydrochar. However, the optimal reaction conditions to reach to appropriate values of these features during co-HTC vary from one work to another given the difference in feedstock composition and the fact that the values of the reaction parameters vary across research investigations. Therefore, it is challenging to get a holistic appreciation of the impact of the processing parameters. As a result, the optimized process conditions for a given feedstock is typically achieved following numerous experimental trials, which causes a waste of time and resources. Also, the results got from a given work cannot be typically well applied to another feedstock, as the reaction is a result of various cross-impact of many features involved. Given this and considering the growing interest in Machine Learning (ML) algorithms models in the field of thermochemical processing of biomass and organic solid waste, the purpose of this work is to examine some data driven ML algorithms for the prediction of fuel properties of hydrochar from co-HTC of SS and lignocellulosic biomass. The hydrochar properties of interest in the current work include carbon content (Ch), H/C ratio (H/Ch), O/C ratio (O/Ch), N/C ratio (N/Ch), higher heating value (HHVh), fuel ratio (FRh), mass yield (MY) and energy yield (EY).

ML refers to a system's ability to acquire and integrate knowledge through large-scale observations, as well as to improve and extend itself by learning new knowledge [11]. Unlike traditional statistics, the core principle of ML is to "let the data speak for themselves," with the human making as few assumptions about the data as possible [12]. However, ML techniques must be used with caution and prudence because they are not a magic bullet and do not replace thoughtful design [11]. The first step in any ML modeling procedure is to establish a hypothesis model that considers information on the nature and characteristics of the process to be modelled. This lowers the possibility of false-positive results and eases the subsequent explanations [12]. A well-designed ML model can provide accurate interpretations to help with important decisions [13].

ML solving problems can be categorized into regression and classification. The problem to address in this work is a regression problem and various ML algorithms are available to approach it. The most widely reported recently in thermochemical processing field include Decision Trees, Supporting Vector Regressor, Artificial Neural Networks, Random Forest (RF), Gradient boosting, and eXtreme Gradient boosting (XGB). In this work, XGB and RF algorithms that implement an ensemble learning approach were examined.

Ensemble learning is a ML approach that combines several base predictors, such as individual learning algorithms, to produce improved prediction in terms of accuracy and stability [14]. Its great accuracy, generalization, and robustness make it a popular ML approach. It is typically divided into boosting (such as XGB) and bagging (such as RF) approaches. XGB is a cutting-edge ensemble learning system that uses the gradient boosting technique together with several decision trees that have been developed in series, with each subsequent decision tree learning and growing from the mistakes of the prior tree [15]. When the subsequent decision trees are sufficiently deep or when there are no longer any error patterns in the prior tree, XGB learning will stop. This algorithm has been reported to be accurate for small to medium-sized structured or tabular data sets [16]. For a regression problem, RF is a bagging ensemble learning method that constructs a given number of regression trees before averaging their individual outputs to generate a final overall prediction. As a result, the overall bias of the algorithm is reduced because there are multiple trees, and each tree is trained on a subset of data. Even if a new data point is added to the dataset, the overall algorithm is hard to be affected because new data may affect one tree, but it is extremely hard to affect all trees.

XGB and RF algorithms have been recently examined and exhibited good prediction results in many works related to hydrothermal processing, including the prediction of higher heating value, and yield of biocrude from hydrothermal liquefaction of wet-biomass [15], the prediction of biocrude yield from hydrothermal liquefaction of organic wastes [16], the prediction of phosphorous content of hydrochar from HTC of SS [17], the multitask prediction of bio-oil properties from hydrothermal liquefaction of biomass [18]. However, to the best of the authors' knowledge, this is the first time ML in general and particularly XGB and RF algorithms are used for the co-HTC processing of SS and lignocellulosic biomass. The accurate predicting models will aid in giving a comprehensive understanding of the effects of the numerous factors that impact the hydrochar properties. The models can also be used for prediction prior to experiments.

2. Methods

2.1. Dataset compilation and pre-processing

To build the dataset, published papers were extensively searched from databases including Web of Sciences, ScienceDirect, Google

Scholar, and Scopus, and downloaded from the journals' websites. After the screening of many peer-review published papers, the papers providing useful information were considered and data was immediately gathered from the included tables or retrieved from the figures in the paper or in the supporting information. The considered dataset in this work includes co-HTC for 20 various SS and 33 various lignocellulosic biomasses, as presented in Table 1. Overall, 221 datapoints were reported for co-HTC conditions. All the raw data are presented in Supplementary Material SM1.

$$C + H + N + O + Ash = 100 \quad (1)$$

$$VM + FCs + Ash = 100 \quad (2)$$

The target fuel properties of the hydrochar considered in this work are presented in Table 2, and include Ch, H/Ch, O/Ch, N/Ch, HHVh, fuel ratio (FRh), mass yield (MY) and energy yield (EY).

From the literature, some of these features maybe evaluated through various formulas. Therefore, HHVh, FRh and EY were calculated using Eq. (3) [35], Eq. (4) and Eq. (5), respectively.

$$HHVh = 0.3491Ch + 1.1783Hh + 0.1034Oh - 0.015Nh - 0.021Ah \quad (3)$$

$$FRh = \frac{FCh}{Vh} \quad (4)$$

Table 1
References for dataset building.

Type of the SS	Type of lignocellulosic biomass	Refs
SS	Cornstalk	[19]
SS	Cellulose	[20]
SS	Xylan	
SS	Lignin	
SS	Water hyacinth	[5]
SS	Pinewood sawdust	[7]
SS	Pinewood sawdust	[21]
SS	Fir sawdust	[22]
SS	Oak sawdust	
SS	Rice Straw	[23]
SS	Banana stalk	[4]
SS	Rice straw	[3]
SS	Orange peel	
SS	Peanut shell	
SS	Fallen leaves	
SS	Sawdust	[24]
SS	Pinewood sawdust	[25]
SS	Wood sawdust	[26]
SS	Corn Stalk	[27]
SS	Pinewood Chip	[28]
Digested SS	Grass Clippings	[29]
Digested SS	Privet Hedge	
Digested SS	Woodchip	
SS biosolid	Corn stover	[30]
Mixture of activated SS and dewatered SS	Sawdust	[31]
Digested SS	Hardwood sawdust	[32]
Digested SS	Softwood sawdust	
Digested SS	Sugarcane bagasse	
Digested SS	Rice husk	
SS	Rice straw	[33]
SS	Sawdust	[34]
SS	Corncob	
SS	Cornstalk	

The data collected include the elemental composition of SS (carbon (Cs), hydrogen (Hs), nitrogen (Ns), oxygen (Os), and sulfur (Ss) contents), the proximate analysis results of SS (volatile matter (Vs), fixed carbon (FCs) and ash (As) contents), the ultimate and proximate analyses results of the lignocellulosic biomass (Cb, Hb, Nb, Ob, Sb, Vb, FCb and Ab), the co-HTC reaction conditions (Reaction temperature (RT), reaction time (Rt), solid loading (SL)), the ratio of SS in the mixture (SSratio), the elemental and proximate analyses results of the hydrochar (Ch, Hh, Nh, Oh, Sh, Vh, FCh and Ah), the mass yield (MY) and energy yield (EY). As these works focused on co-HTC, the HTC conducted in these works with SS alone for control was considered as co-HTC with SSratio = 100%. All the data are on dry basis (wt.%, db), then Eq. (1) and Eq. (2) were verified.

Table 2
Output variables considered in the current work.

Feature	Name in the manuscript
Carbon content in the hydrochar	Ch (wt.%)
Hydrogen to carbon ratio of the hydrochar	H/Ch
Oxygen to carbon ratio of the hydrochar	O/Ch
Nitrogen to carbon ratio of the hydrochar	N/Ch
Higher heating value of the hydrochar	HHVh (MJ/kg)
Fuel ratio of the hydrochar	FRh
Mass yield of the hydrochar	MY (wt.%)
Energy yield of the hydrochar	EY (%)

$$EY = \frac{HHVh}{HHVmix} \times MY \quad (5)$$

For the prediction, three (03) various configurations of the input features were assessed for each of the outputs. These configurations include the data of ultimate analysis alone, proximate analysis alone, and both ultimate and proximate analyses data. The number of data points retained for each configuration for a given output feature are listed in Table 3.

2.2. Hyper-parameter turning and model accuracy evaluation

XGB and RF are the two algorithms retained for this work. The functioning of XGB algorithm is thoroughly described in some recent works [15,36] and more details about the RF algorithm can also be found elsewhere [17,37]. In this work, the models' implementation was conducted via Scikit-learn python library.

(https://scikit-learn.org/) supported on Anaconda (https://www.anaconda.com/). For both algorithms, only the number of trees (n_estimators) and the maximum depth of trees (max_depth) were optimized. The other parameters were left to their default values (xgboost version 1.6.2 and scikit-learn version 1.1.2).

The hyperparameters' turning optimization was conducted using the "hyperopt" library (available optimization algorithm library that was integrated in python) with lower RMSE (Root Means Square Error) as the termination criterion.

Before developing the models, the dataset was randomly split into two subsets, including 80% for training and 20% for testing. The accuracy of the models for both training and testing was evaluated using the Root Means Square Error (RMSE) (Eq. (6)) and the square of the correlation coefficient (R^2) (Eq. (7)).

$$RMSE = \sqrt{\frac{1}{K}\sum_{j=1}^{K}\left(Y_{j,p} - Y_{j,r}\right)^2} \quad (6)$$

Table 3
Dataset configuration employed for the model building.

Input configurations	Output features	Number of datapoints
Ultimate analysis + SSratio + HTC conditions	Ch, H/Ch, O/Ch, N/Ch and HHVh	188
	FRh	155
	MY and EY	116
Proximate analysis + SSratio + HTC conditions	Ch, H/Ch, O/Ch, N/Ch and HHVh	156
	FRh	188
	MY and EY	92
Ultimate and proximate analyses + SSratio + HTC conditions	Ch, H/Ch, O/Ch, N/Ch and HHVh	156
	FRh	155
	MY and EY	89

$$R^2 = \frac{\sum_{j=1}^{K}\left(Y_{j,p} - Y_{p,avg}\right) \times \left(Y_{j,r} - Y_{r,avg}\right)}{\sqrt{\left[\sum_{j=1}^{K}\left(Y_{j,p} - Y_{p,avg}\right)^2\right] \times \left[\sum_{j=1}^{K}\left(Y_{j,r} - Y_{r,avg}\right)^2\right]}} \quad (7)$$

K is the number of measured values; $Y_{j,p}$ is the predicted value; $Y_{j,r}$ is the real value measured; $Y_{p,avg}$ is the mean value of the predicted data vector; and $Y_{r,avg}$ is the mean value of the measured data vector.

2.3. Analysis of the impact of input features on targets

Once the models with optimum hyper-parameters were reached and their performances were confirmed, partial importance and partial dependance analyses were conducted to point out the impact of each input on the output. SHAP (Shapley Additive exPlanations), which is a game theory-based method was employed for the partial importance analysis. This method available in the scikit-learn toolbox treats each input variable value as a player in a game where the profit is the prediction output. The SHAP values then tell us how to proportionally distribute the profit among the players. The partial dependence plots (PDP) were also plotted from the prediction model to show the specific average contribution of the most impactful input features. PDP displays the marginal impact of one or two input features on the outcome of a model. The mathematics behind the methods of PDP are well-described elsewhere [38].

3. Results and discussion

3.1. Dataset characterization

The ranges of features of the SS, the lignocellulosic biomass, and the hydrochar are presented in Table S1 of the Supplementary Material SM2 and also represented in Fig. 1(a–g), and the reaction conditions explored for co-HTC are presented in Fig. 1h. From Fig. 1a and b, it can be observed that compared to SS, lignocellulosic biomasses exhibit higher carbon, oxygen, fixed carbon and volatile matter contents, while overall, their ash and nitrogen contents are lower. The high ash content of SS is attributed to inorganic species [39]. The high N of SS comes from the proteins that constitute a main compounds' group for SS. The higher value of Cb, Ob, Vb and FCb compared to Cs, Os, Vs and FCs is understandable given that lignocellulosic biomass contains relative high contents of lignin, cellulose, hemicellulose and extractives [40], while in SS, relatively low cellulose and lignin contents have been reported besides the high ash content [2]. The fixed carbon content of the hydrochar is improved when compared to both SS and biomass. This ensures an improved firing temperature and flame stability during combustion of the hydrochar, when compared to SS and biomass [10]. Vh and Ch are reduced when compared to Vb and Cb, while they are improved when compared to Vs and Cs. It can also be observed that the variation ranges of the elemental compositions and proximate analysis results of SS are larger than those for features of the lignocellulosic biomasses. This can be justified by the fact that the composition of SS is highly variable and depends on many various factors such as the seasons, the origins of the wastewater, the purifying processes used for the wastewater and the conditioning and stabilizing operations employed for the SS [2,41,42]. For e.g., it is reported that communal.

wastewater has a higher content of pollutants than household wastewater due to the contribution of polluting compounds from industry [43]. Some works also reported that primary SS contains 5–27.58 wt% total dry solids with 18.8–80 wt% volatile solid, 2–30 wt% protein, and 8–15 wt% cellulose [42,44], while secondary SS contains 0.8–25.36 wt% total dry solids with 30.88–68 wt% volatile solid, 15–41 wt% protein, and 7–9.7% cellulose [44]. On average, dewatered SS contains 50–70% organic matter, 30–50% mineral components, and 3.4–4.0% nitrogen [41].

Fig. 1d clearly shows that the HHVs is lower than HHVb, and the mixing of the feedstocks help to adjust the HHVmix of the mixture keeping it near the biomass structure as confirmed by the Van Krevelen diagram of Fig. 1e. From this diagram, it can be observed that the addition of biomass pushes the mixture into the region of biomass and going near to the structure of peat, while SS alone is mostly out of the region with higher H/C and O/C ratios. The reduced H/C and O/C ratios of mixtures will play a great role during HTC process and may explain the further reduced ratios observed for the hydrochars. The lowered H/C and O/C ratios will result in the reduction of smoke and water vapor during the combustion of the hydrochar [45]. The data for the mixture and the hydrochar in Fig. 1e also reveals that dehydration occurs more than decarboxylation and demethylation during co-HTC. This agrees with some recent reports that mentioned dehydration and depolymerization to be among the top reaction promoted during HTC of high cellulose feedstock [46,47], probably promoted by the acidic intermediate compounds such as organic acids formed during the reaction.

Fig. 1f depicts the N/C ratios of the various materials. It can be seen that SS exhibits a significantly higher N/C ratio (N/Cs) when compared to biomass (N/Cb). Theoretically, this can be attributed to the fact that Cs <Cb and Ns>Nb, as observed in Fig. 1a and b. Practically, lower N/C ratio is suitable for fuel application while higher N/C ratio traduces lower C content that may stimulate the release of microbial N and thus increase the crop-available N when the hydrochar is used for soil amendment [48]. The mixed feedstock as well as the derived hydrochar exhibit decreased N/C ratios (N/Cmix and N/Ch) but these ratios sill higher than that of the lignocellulosic biomass (N/Cb). N/Ch is more concentrated in a narrow range while variation range of N/Cmix is the largest.

As depicted in Fig. 1g, the fuel ratio of SS (FRs) is located between 0.023 and 0.14, and FRb is mainly located between 0.017 and 0.25. These values are lower than 0.33 and thus, both the SS and most of the biomass examined in co-HTC are non-stable solid fuels with a half-life <100 years [49]. After the co-HTC, some values of the FRh were improved to reach more than 0.33 as it can be observed from Fig. 1g. Overall, the addition of biomass to SS help to improve the properties of the mixture relatively to SS, but the resulting properties still lower than those of the hydrochar. Therefore, co-HTC is required for further improvement.

3.2. Preliminary analysis before prediction

Prior to the modelling, the Pearson correlation coefficients (PCCs) between all variables involved in the modelling process were evaluated and presented in Fig. 2a. It is revealed that between inputs and outputs, only SSratio exhibited higher PCC (>0.5) with Ch, H/Ch, N/Ch and HHVh. This instructs that SSratio is an important factor to estimate these features. EY exhibits significant PCC (0.72 and 0.6) with SL and Cb, respectively. MY exhibits significant PCC (0.58) with SL. However, the squares these PCCs are lower to provide accurate prediction of These features.

The distributions of the output features are depicted in Fig. 2b. It is noticed that nearly Gaussian distribution tendencies can be seen for all of the output features, indicating that data close to the mean are more likely to occur than data far from the mean. This normal distribution tendency suggests the possibility of existence of accurate models for predicting these properties.

3.3. Machine learning modeling

The optimum parameters for all configurations explored are presented in Table S2. The hyperparameter tuning process of the best configuration revealed are presented in Fig. 3(a–h) and the properties and performance of the best optimized models obtained are summarized in Table 4. The performance of the modelling can be assessed on two ways including the impact of the co-HTC features and the impact of the

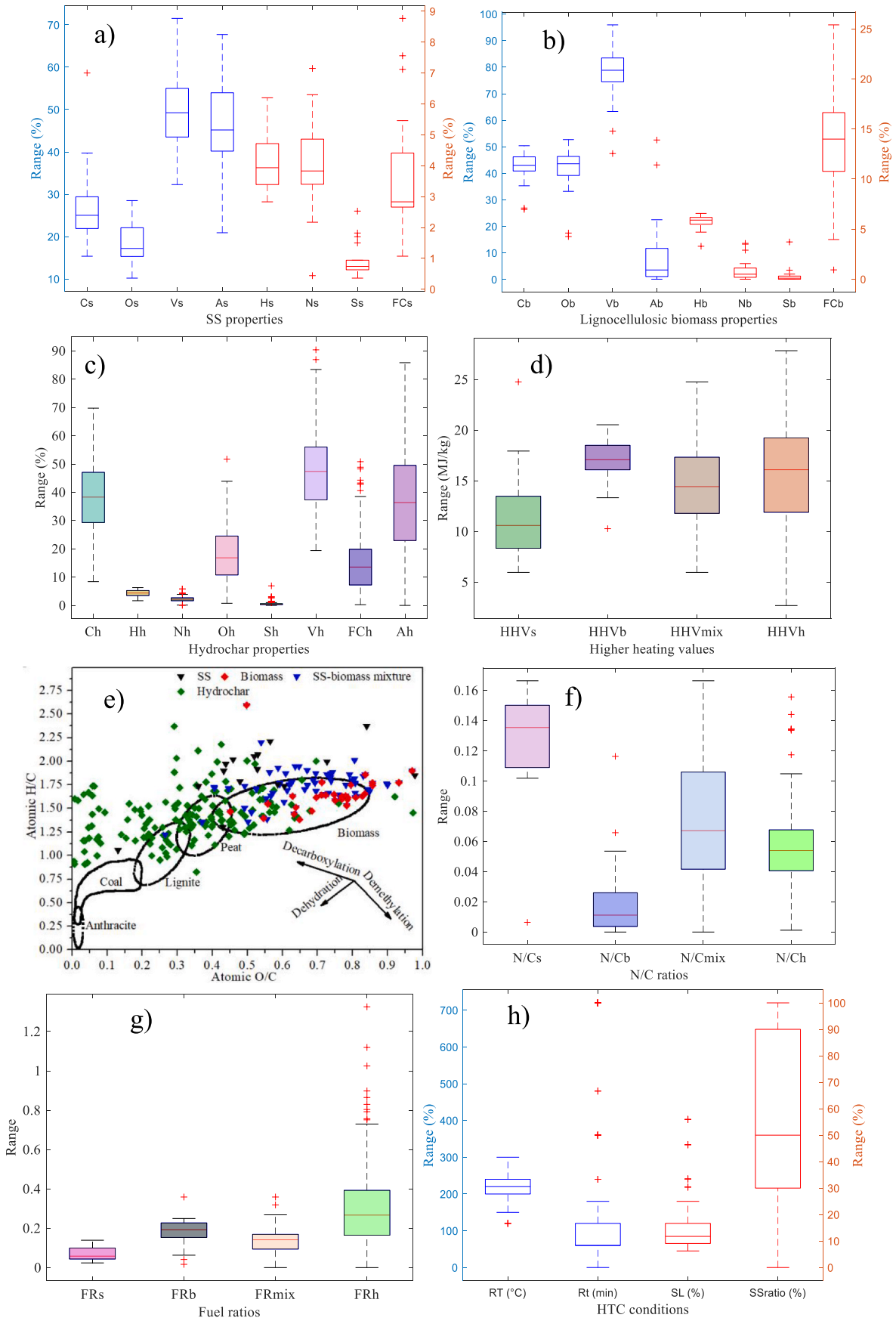

Fig. 1. Characterization of the dataset of the SS, biomass, hydrochar and HTC conditions (a–h).

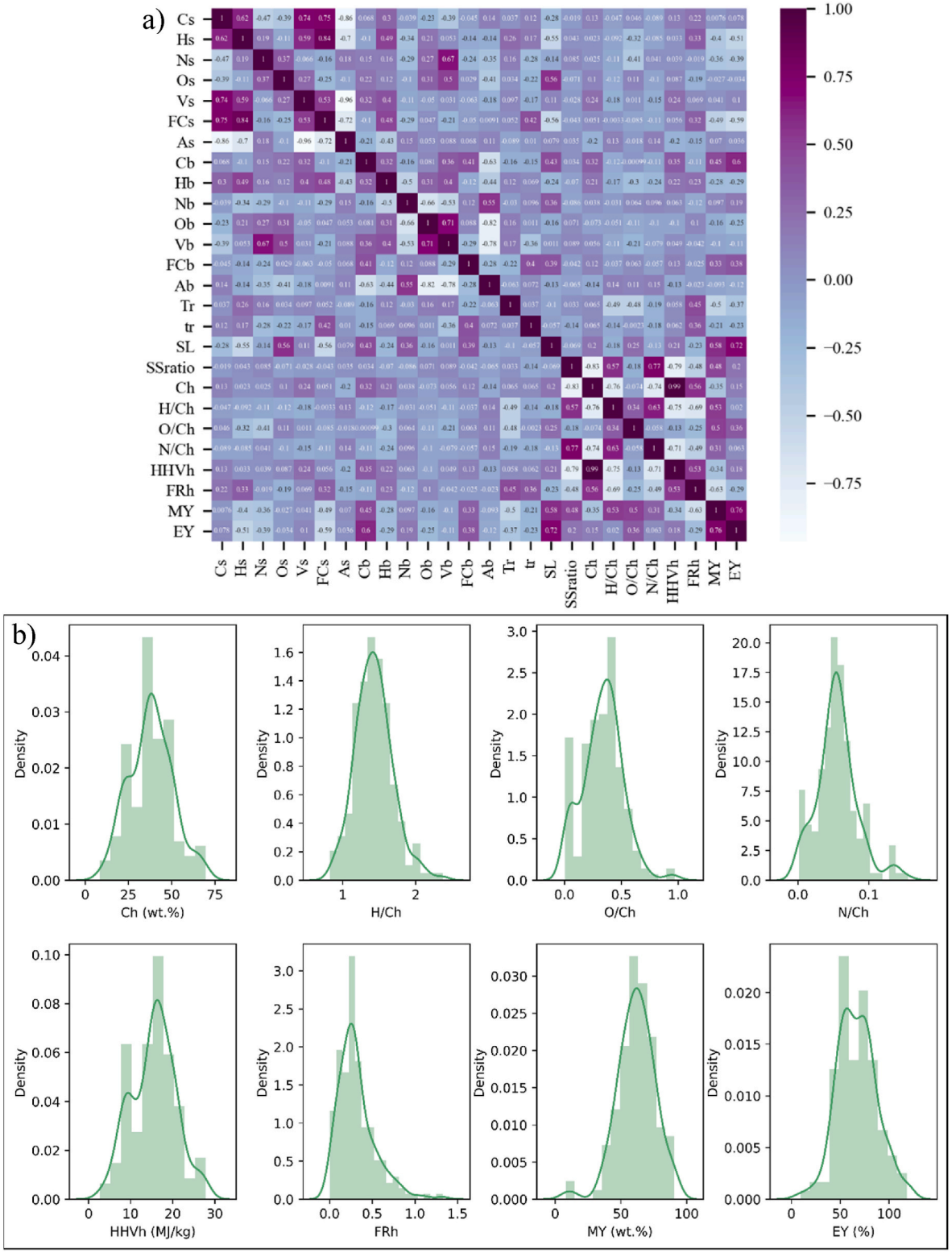

Fig. 2. Pearson Correlation coefficients among variables (a) and distribution of the target variables (b).

ML algorithms.

On the side of the co-HTC features, the elemental compositions of SS and biomass combined with SSratio and HTC conditions exhibited the best performances for the prediction of Ch, H/Ch, O/Ch, N/Ch, HHVh, MY and EY, while for the prediction of FRh, the proximate analysis results of SS and biomass combined with SS ratio and HTC conditions was the best. On the side of examined ML algorithms, RF was best in predicting H/Ch, N/Ch and FRh, while XGB provided accurate prediction for Ch, O/Ch, HHVh, MY and EY. Some other works also found XGB algorithm more accurate than RF for the prediction of HHV and yield of biocrudes from hydrothermal liquefaction of wet-biomass [15], and for the prediction of municipal solid waste generation in China [50], while in the work of Cheng et al. [16], RF was slightly better than XGB for the prediction of biocrude yield from hydrothermal liquefaction of organic

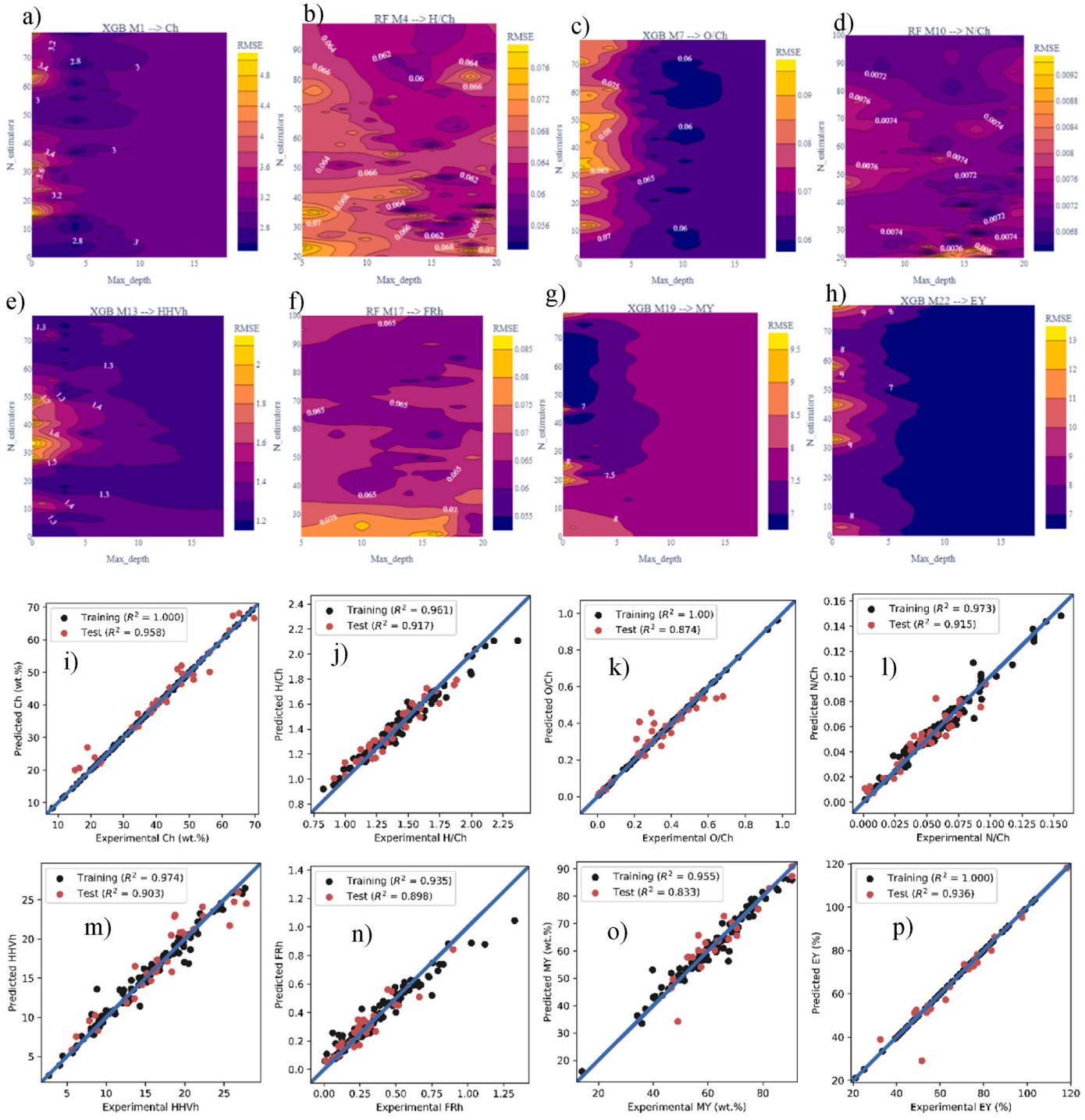

Fig. 3. Hyperparameters' optimization step (a–h) and performances plots (i–p) of the best models obtained for the prediction.

wastes.

The correlation plots between the predicted and experimental values of the various outputs for the training and test datasets are depicted in Fig. 3(i–p). The blue line (y = x) indicates that the prediction values equal to the actual value, and the closer of the dots to this line reflects the better prediction performance. As it can be seen, all the prediction vs. experimental training and test points exhibits good performances. All models show a higher prediction accuracy on the training dataset when compared to that observed for the testing dataset, as previously noticed [18]. This is due to the fact the model is not fit directly to the test data, and the effect of the test is to de-tune the model to minimize over fitting [16].

The findings from this modeling implies that XGB and RF algorithms can be effectively applied for model development for the prediction of Ch, H/Ch, O/Ch, N/Ch, HHVh, FRh, MY and EY of hydrochar produced from the co-HTC of SS and lignocellulosic biomass, based on feedstocks characteristics (ultimate and proximate analyses properties), SS ratio in the co-feedstock and co-HTC conditions (reaction temperature, reaction time, solid loading) as input variables. The accuracy of a model can be increased by choosing more pertinent input variables, while adding unnecessary input variables might easily mislead the model. Referring to the feedstocks properties, elemental analysis results are found relevant

Table 4
Best results of hyper-parameter optimization for various targets.

Models	Inputs	Output	RF algorithm			XGB algorithm		
			Maxdepth	N_estimators	RMSE	Maxdepth	N_estimators	RMSE
M1	Cs, Hs, Ns, Os, Cb, Hb, Nb, Ob, RT, Rt, SL, SSratio	Ch (wt.%)	8	40	3.670	**5**	**79**	**2.543**
M4	Cs, Hs, Ns, Os, Cb, Hb, Nb, Ob, RT, Rt, SL, SSratio	H/Ch	**13**	**36**	**0.053**	2	30	0.064
M7	Cs, Hs, Ns, Os, Cb, Hb, Nb, Ob, RT, Rt, SL, SSratio	O/Ch	20	22	0.074	**10**	**25**	**0.058**
M10	Cs, Hs, Ns, Os, Cb, Hb, Nb, Ob, RT, Rt, SL, SSratio	N/Ch	**18**	**22**	**0.006**	10	19	0.008
M13	Cs, Hs, Ns, Os, Cb, Hb, Nb, Ob, RT, Rt, SL, SSratio	HHVh (MJ/kg)	18	52	1.567	**3**	**54**	**1.174**
M17	Vs, FCs, As, Vb, FCb, Ab, RT, Rt, SL, SSratio	FR	**18**	**85**	**0.054**	3	77	0.066
M19	Cs, Hs, Ns, Os, Cb, Hb, Nb, Ob, RT, Rt, SL, SSratio	MY (wt.%)	10	44	8.082	**2**	**61**	**6.551**
M22	Cs, Hs, Ns, Os, Cb, Hb, Nb, Ob, RT, Rt, SL, SSratio	EY (%)	18	37	7.065	**8**	**49**	**6.117**

features for the prediction of Ch, H/Ch, O/Ch, N/Ch, HHVh, MY and EY while the proximate analysis properties are the most relevant features for the prediction of FRh. The superiority of XGB over RF for some outputs and the superiority of RF over XGB for other outputs can be justified by the mathematics of each algorithm and the properties of the data.

3.4. Input features' partial importance and interpretation of partial dependance analysis

A scientist who wants to learn more about a model's operation needs more information than simply evaluating its accuracy. Therefore, model explainability is crucial in the field of machine learning because it provides insight into how different input features affect prediction outcomes and identifies the most impactful features. For this goal, we used the SHAP approach. The partial importance quantified by the mean absolute SHAP value are quantified and grouped in four (04) categories of input features as presented in Fig. 4 and also presented with raw SHAP values for each input feature in Fig. 5(a–b) and Figs. S1 (a-f).

The mean absolute SHAP values (bars in green color in Fig. 5(a–b) and Figs. S1 (a-f)) indicate the degree of impact without specifying if the impact is negative or positive. For the SHAP values (distribution in red and blue in Fig. 5(a–b) and Figs. S1 (a-f)), the horizontal position indicates the degree and the direction of impact (lower or higher, negative or positive) of a given input variable. Red color indicates a high value of the variable, while the blue color indicates a low value.

To provide further insight into the features' impacts, partial dependence plots (PDP) were reported for the most impactful features and presented in Figs. 6 and 7, and Figs. S2 and Fig. S3 of the supporting information. In fact, the functional relationship between one (one-way PDP) or two (two-way PDP) input variables and the prediction is represented by a PDP, which can also demonstrate whether the relationship between the target and the input variable is linear, monotonic, or more complex. While two-way PDP (Fig. 7 and Fig. S3) helps to look for interactions between two input variables of interest, one-way PDP (Fig. 6 and Figs. S2) demonstrates how the prediction depends on the values of one input variable of interest.

As presented in Fig. 4, SSratio followed by the HTC conditions are the most impactful factors on H/Ch and N/Ch. SSratio is more impactful on N/Ch than H/Ch while HTC conditions are more impactful on H/Ch than N/Ch. The biomass properties are the most impactful for the O/Ch, and their impacts on the various output features decreased in the order of O/Ch, MY, Ch, H/Ch, FRh, HHVh, N/Ch and EY. SS properties are the most impactful factors on the Ch, HHVh, MY and EY. The biomass properties impact more on MY than EY, while the impacts of SSratio and HTC conditions on these features are almost the same. For the FRh, HTC conditions are the most impactful, followed by the SS ratio. The impact of SS properties and biomass properties are almost the same.

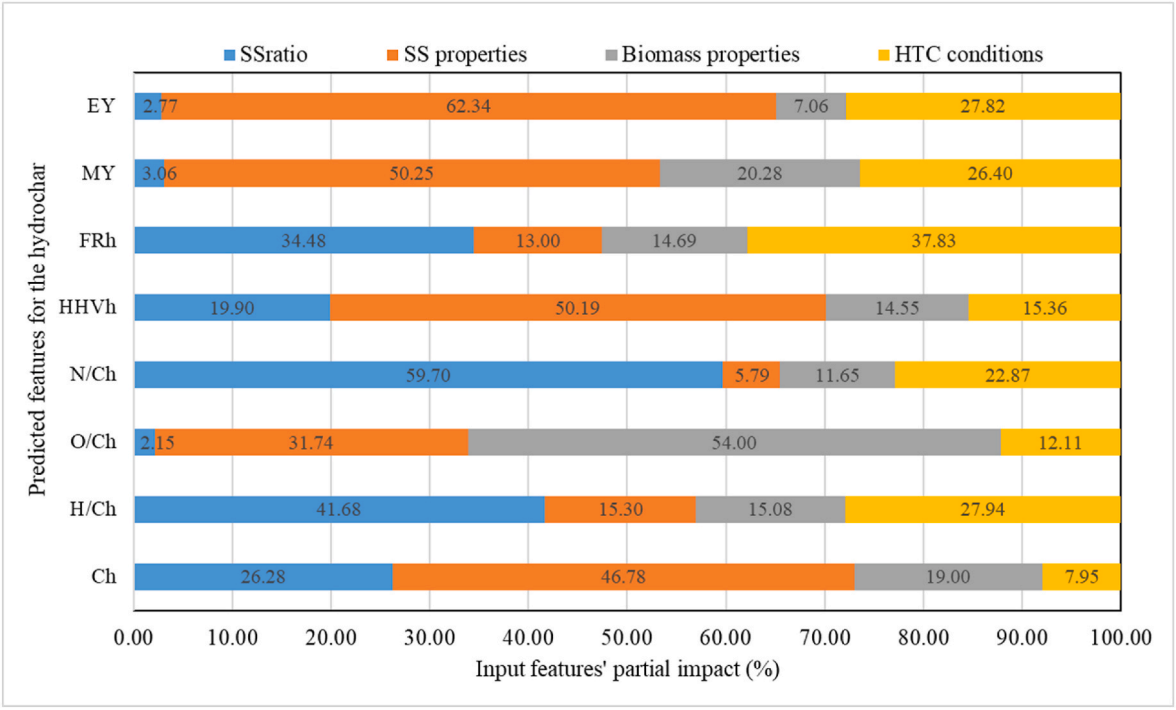

Fig. 4. Partial impact of features.

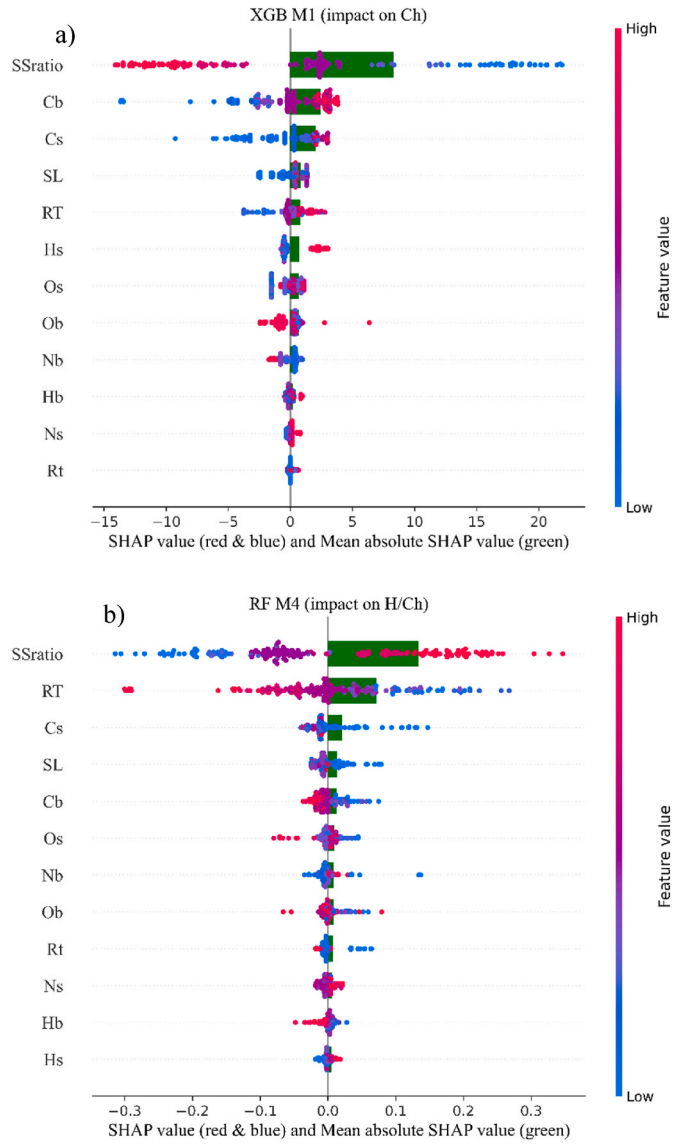

Fig. 5. Input features' partial impact on the various outputs: a) Ch, and b) H/Ch.

As it can be seen from Fig. 5 and Figs. S1, SSratio is the most impactful factor for many outputs. Fig. 5a shows that SSratio is the most impactful feature on Ch, followed by Cb, Cs, SL, Cb. Higher values of SSratio exhibits significant negative impact on Ch, while lower values of SSratio exhibits low positive impact on Ch. Opposite effect is observed for Cb, Cs, SL, RT. Reaction time (Rt) exhibits almost no effect on the Ch. The PDP plot in Fig. 7a confirms that Ch increased with both Cs and Cb, while Fig. 7b reveals that for Ch, SSratio is more impactful than RT, and Ch increases with RT while decreases with SSratio. Similar impact properties are observed for HHVh (Fig. S1c). This is probably due to Eq. (3) that was used to evaluate HHVh and in which Ch has a great share.

Fig. 5b shows that SSratio is the most impactful features on H/Ch, followed by RT, Cs, Os, SL. Higher values of SSratio exhibits significant positive impact on H/Ch. Overall, opposite impact as compared to the impact on Ch was observed for many features including RT, Cs, Cb, Os. This is understandable, as higher Ch would lower H/Ch. Although higher SSratio positively impact on the H/Ch and N/Ch ratio, its impact on the O/Ch is negative. This is confirmed by the PDP plots depicted in Figs. S2(b, c, d). This can be attributed to two reasons. On one hand, it can be assigned to the lower Os and higher Ns, relatively to Ob and Nb, as presented in Fig. 1(a and b). Therefore, higher SSratio would bring lower oxygen in the reaction system that would lead to lower Oh and thus lower O/Ch. On the other hand, the presence of ammonia-N in SS could lower the Oh via C═O conversion into C–N and C═N.

Fig. S1b states that the N/Ch is more dependent on SSratio, RT, Ns, and Nb. Higher Ns showed positive impact on N/Ch. This agrees with the impact observed for the SSratio, as higher SSratio will bring more Ns to the solid in the reactor. Higher values of RT impact negatively on the N/Ch. This can be assigned on one hand to the increase carbonization with increasing temperature that leads to increase Ch, and on the other hand, to the devolatilization that occurs with increasing temperature and can release a part of nitrogen in the form of gas or in the liquid phase. It can also be observed that compared to values of Ns, higher values or lower values of Nb would impact more N/Ch. This is confirmed by the two-PDP presented in Fig. 7c exhibits an increase of N/Ch with increasing of both Ns and Nb. However, the increase of N/Ch is more pronounced with increasing Nb. Same trend is observed in Fig. 7(d and e). This is probably related to the predominant organic-nature of Nb that may lead to more N in the hydrochar, while Ns contains more inorganic-N that is easily releasable either in water phase or in gas phase. A recent work also noticed that the resolidification of N in the aqueous phase into solid phase via polymerization and heterogeneous bonding reaction was enhanced with increased corn stalk amount in the reaction system of co-HTC with SS [19]. Fig. 7(d and e) also show a sharp decrease of N/Ch at temperatures around 175 °C and a slight decrease is maintained for temperatures above. However, Fig. 7f reveals that the effect of temperature on N/Ch is related to SSratio. Higher SSratio at lower temperature leads to high N/Ch, while the N/Ch significantly decreases for temperature above 235 °C even at high SS ratio. This confirms that the addition of lignocellulosic biomass is a good way to reduce N/Ch.

For FRh (Fig. S1d), HTC reaction conditions are the most impactful features, followed by FCs and FCb. Higher values of SSratio negatively impact FRh, as confirmed by the PDP in Fig. S2f. This is attributed to the fact that carbon is more fixed in lignocellulosic biomass than in SS. The impact distribution observed for RT is partly ascribed to the devolatilization that would reduce the volatile matter in the solid hydrochar and thus leads to a concentrated FCh resulting in increased FRh according to Eq. (4). In difference to the other models, the reaction time (Rt) appeared as the third most influential factor on FRh. Longer reaction time may promote FRh and thus the stability of the hydrochar through an increase of the FCh and reduction of the Vh as recently noticed [51].

Reaction temperature is the most impactful factor among the various HTC conditions and exhibits a significant effect on various properties of the hydrochar. Higher reaction temperature and longer reaction time may lead to higher reaction severity of the dehydration, hydrolysis, decarboxylation and higher breakdown of the feedstock, resulting in increased Ch, HHVh and FRh [45,52]. As it can be seen from Fig. 5b and Fig. S1a, RT is slightly more impactful on O/Ch than H/Ch, claiming that compared to dehydration reactions, decarboxylation reactions are more governed by the HTC temperature during co-HTC of SS and lignocellulosic biomass. This corroborates the finding of Borbolla-Gaxiola et al. [51] when these authors employed multi-variate and multi-response analysis of HTC of food waste for temperatures in 180–260 °C. The results depicted in Fig. 6 let speculate that during the co-HTC, the carbonization reactions are initiated from around 180 °C.

The impact of reaction time on various outputs is presented in Fig. 6 (g–l). Prolonged reaction time may promote the decomposition of cellulose and hemicellulose [53], lowering the amount of oxygen-containing surface functionalities on the hydrochar, and this effect would be more enhanced at higher temperature [54]. The longer reaction time may also promote the decomposition of aliphatics, alcohols, sugars, and aromatics in the water and the integration of the derivatives compounds within the hydrochar. This can justify the improved FRh with increased reaction time (Fig. 6l). The reduction of Ch at excess reaction time is probably due to the enhanced decomposition of compounds that are directed to the liquid phase at lower temperature or to the gas phase at high temperature.

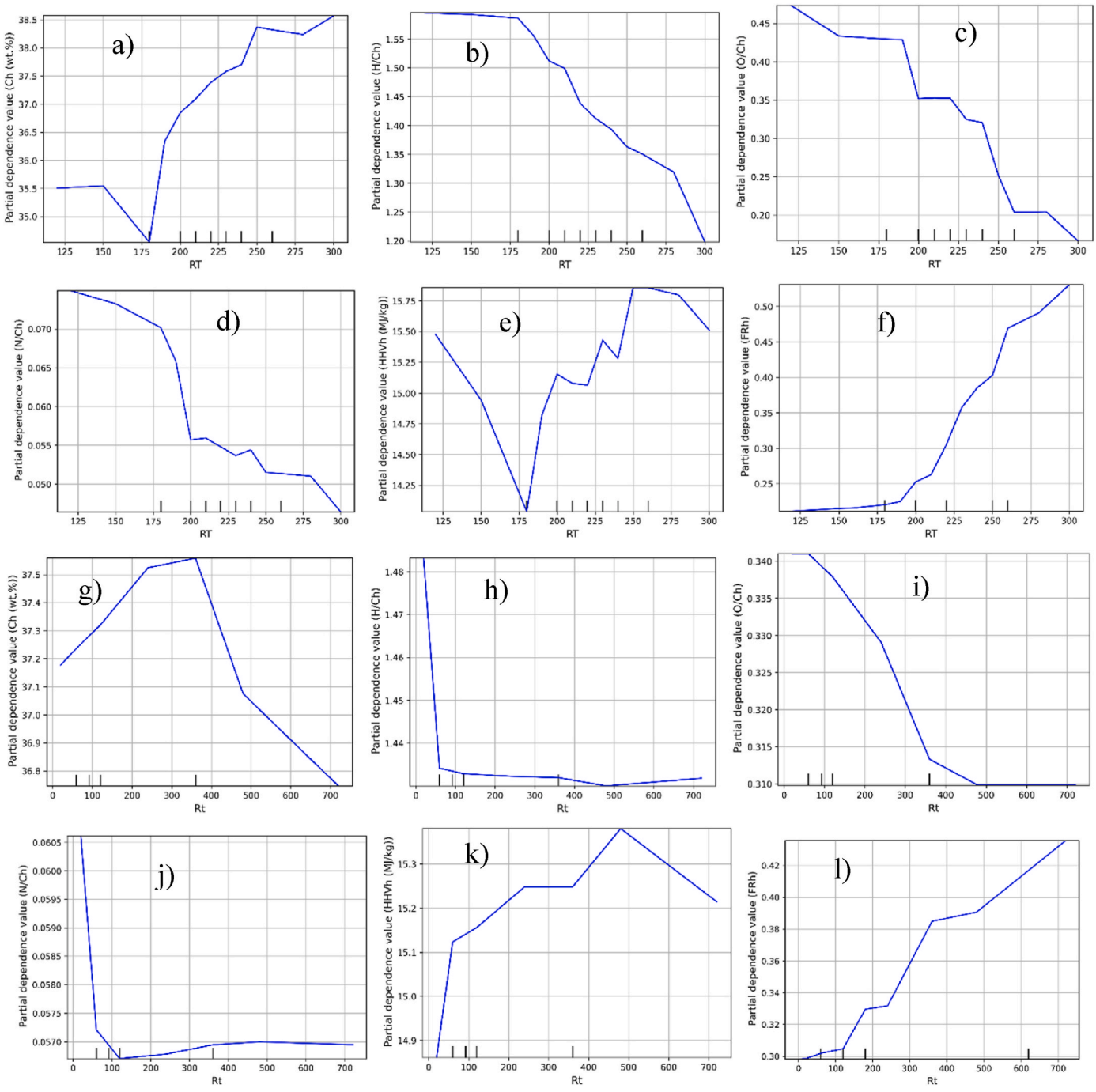

Fig. 6. One-way Partial Dependance Plots for reaction temperature (RT) and reaction time (Rt) on various outputs.

The impact of solid loading on various outputs is presented in Fig. S2 (i-o) and can be attributed to two reasons. On one hand, the lower liquid content may facilitate the generation of secondary char and improve the reaction severity due to the high acidity in the reaction system caused by the concentrated intermediates. On the other hand, lower liquid content inhibits the relative interactions among molecules of the feedstock and water, and that may suppress the dissolution of some compounds of the feedstock. These observations are in line with previous findings which reported that compared to liquid-based HTC process, vapor-based process further improved the degree of coalification and the stability of the hydrochar from dairy manure [55]. Increased solid loading for a high ratio of SS (high-protein content in the co-feedstock) could improve the alkalinity in the reaction system via the deamination of the proteins while at lower SS ratio increase solid loading may improve the acidity of the reaction system via the decomposition of carbohydrate compounds. These mechanisms may result in the change of the pH of the reaction system that may lead to some further catalytic activities. Therefore, the solid loading should be made in accordance with the properties of the feedstock, the reaction temperature, and the expected use of the hydrochar.

Overall, the observations from the PDP are in line with those from SHAP method analysis. SSratio exhibited monotonic relationship with almost all features (Figs. S2(a-g)) except EY (Fig. S2h). Increasing SSratio decreases Ch, O/Ch, HHVh, and FRh, while increasing H/Ch, N/Ch, and MY. The complex relationship between SSratio and EY maybe related to the properties of mixture feedstocks (biomass and SS) that

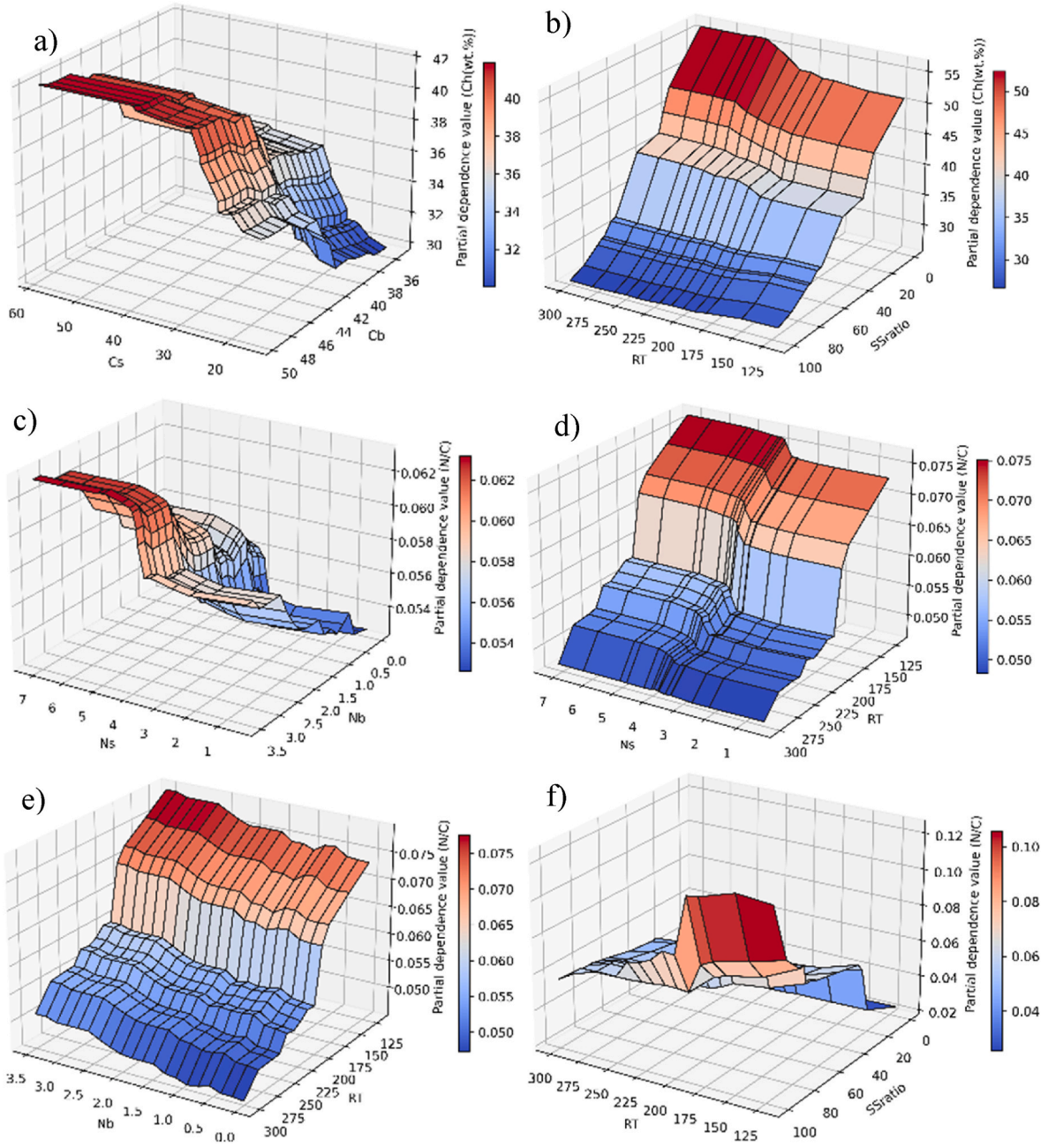

Fig. 7. Two-way Partial Dependance Plots: a) dependance of Ch on Cs and Cb, b) dependance of Ch on RT and SSratio, c) dependance of N/Ch on Ns and Nb, d) dependance of N/Ch on RT and SSratio, e) dependance of N/Ch on Ns and RT, f) dependance of N/Ch on Nb and RT.

intervenes in Eq. (5). SS contains lower carbon, hydrogen and oxygen contents than biomass, but SS properties are the most impactful factor on Ch and HHVh. In fact, a feature can positively impact on an output but this positive impact can be inhibited by the impact of other features, as the HTC reaction is a result of various cross-impact of many features involved. Therefore, the impacts of the various inputs could not be foreseen and the partial dependance analysis has been a valuable tool.

3.5. Online graphical user interface for prediction of hydrochar properties

To easy the use of our solution by other researchers, we have developed an online graphical user interface and some screenshots are presented in Fig. 8. This prediction tool is developed basing on the best models retained from the prediction and can be used from the following link: (https://strategefil-cohtc-cohtc-fuel-n2lxgw.streamlit.app/). The code behind is based on XGB and RF algorithms implemented with python programming language and Scikit-learn library. Researchers could enter the properties of SS and lignocellulosic biomass, the co-HTC conditions and the ratio of SS, and the developed online tool will help to predict the various properties of the hydrochar.

3.6. Outlook of the current study

The models developed in this study can be used to instruct researchers for the co-processing of sewage sludge and lignocellulosic biomass to produce hydrochar with desirable properties such as mass yield, C content, H/C ratio, O/C ratio, N/C ratio, fuel ratio, higher heating value, and energy yield. This could greatly help save time and resources usually allocated for many trials experiments. Despite the good prediction results observed in this work, the following additional

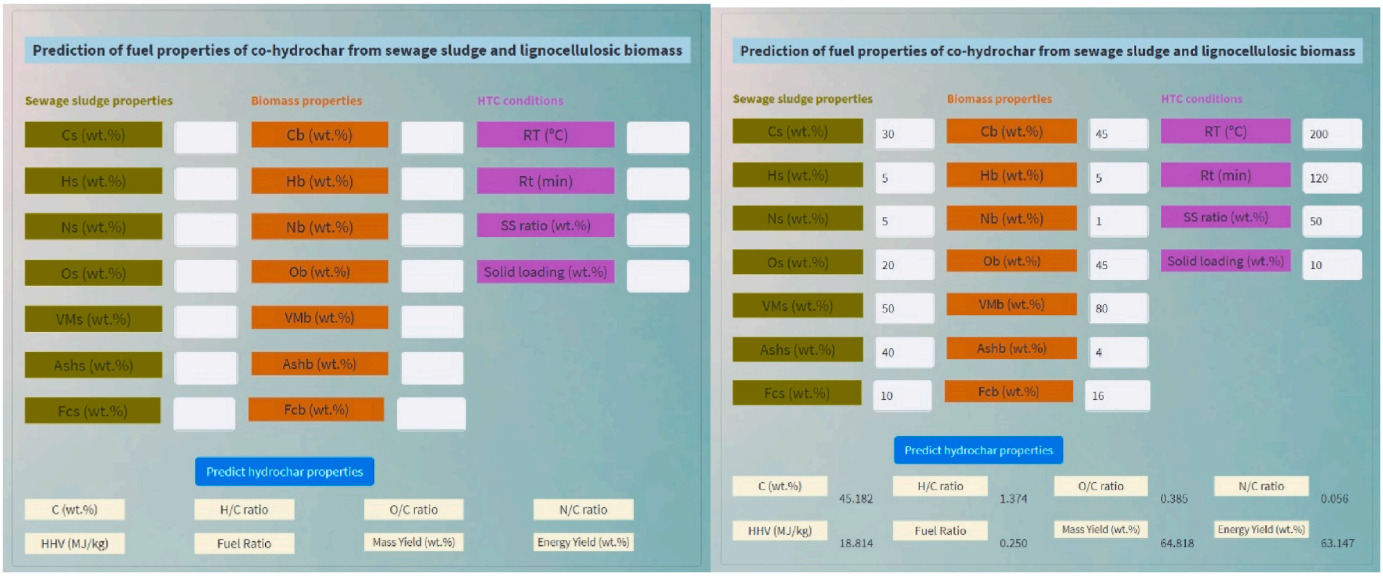

Fig. 8. Screenshots of the online graphical user interface for the prediction of co-hydrochar properties.

considerations should be made to enhance the generalization of the models.

i. More data should be collected to increase the size of the dataset.
ii. While the input parameters considered are reasonable, other variables such as catalyst types and loading amounts should be considered to enhance model generalization. The structural analysis results (contents of cellulose, hemicellulose, lignin, and proteins) of the sewage sludge and biomass can also be examined.
iii. The output variables can also be expanded. As the hydrochar is also used for carbon material synthesis, surface properties (such as surface area, pore volume, pore size, and density) and chemical O- and N-functionalities of the hydrochar can be considered.
iv. The contents of heavy metals with potential risk of ecotoxicity can be considered.

4. Conclusion

The objective of this work was to accurately estimate the fuel properties of hydrochar produced from co-HTC of SS and lignocellulosic biomass and to offer insights into the impact of the process parameters. XGB and RF as machine learning algorithms were used to investigate features such as the elemental and proximate analyses of sewage sludge, the elemental and proximate analyses of lignocellulosic biomass, the SS ratio of the dry matter in the reaction system, and the co-HTC conditions (reaction temperature, reaction time, and solid loading). When comparing input features, it can be seen that the elemental compositions of SS and biomass combined with SS ratio and HTC conditions were sufficient for an accurate prediction of Ch, H/Ch, O/Ch, N/Ch, HHVh, MY, and EY, whereas the best prediction of FRh was obtained from the proximate analysis results of SS and biomass combined with SS ratio and HTC conditions. XGB outperformed RF in the prediction of Ch, O/Ch, HHVh, MY, and EY, while RF excelled in the prediction of H/Ch, N/Ch, and FRh. The partial importance analysis revealed that biomass properties have the greatest impact on O/Ch, while SS properties have the greatest impact on Ch, HHVh, MY, and EY. The FRh is the only feature where HTC conditions have the greatest impact.

Credit author statement

Oraléou Sangué Djandja: Conceptualization; Investigation; Methodology; Software; Data curation; Formal analysis; Writing – original draft. Shimin Kang: Funding acquisition; Conceptualization; Methodology; Visualization; Investigation; Supervision; Validation; Writing – review & editing. Zizhi Huang, Junqiao Li, Jiaqi Feng & Zaiming Tan: Methodology; Software; Data curation. Adekunlé Akim Salami & Bachirou Guene Lougou: Conceptualization; Methodology; Software; Visualization; Writing – review & editing.

Declaration of competing interest

The authors declare that they have no known competing financial interests or personal relationships that could have appeared to influence the work reported in this paper.

Data availability

Data will be made available on request.

Acknowledgments

This work was supported by funding from the Guangdong Provincial Key Laboratory of Distributed Energy Systems (2020B1212060075), the Guangdong Innovation Research Team for Higher Education (2017KCXTD030), the Characteristic Innovation Project of Guangdong Provincial Department of Education (2021KTSCX133), the Dongguan Sci-tech Commissioner Project (20211800500282), GuangDong Basic and Applied Basic Research Foundation (2022A1515 010578) and the College Students' Climbing Plan of Guangdong Province (pdjh2019b0484; pdjh2023a0507).

Appendix A. Supplementary data

Supplementary data related to this article can be found at https://doi.org/10.1016/j.energy.2023.126968.

References

[1] Frankl Paolo. COP26, bioenergy and IEA net zero by 2050 roadmap. 2021.
[2] Djandja OS, Yin L, Wang Z, Duan P. From wastewater treatment to resources recovery through hydrothermal treatments of municipal sewage sludge : a critical review. Process Saf Environ Protect 2021;151:101–27. https://doi.org/10.1016/j.psep.2021.05.006.
[3] He C, Zhang Z, Ge C, Liu W, Tang Y, Zhuang X, et al. Synergistic effect of hydrothermal co-carbonization of sewage sludge with fruit and agricultural wastes

on hydrochar fuel quality and combustion behavior. Waste Manag 2019;100: 171–81. https://doi.org/10.1016/j.wasman.2019.09.018.
[4] Zhang C, Zheng C, Ma X, Zhou Y, Wu J. Engineering Co-hydrothermal carbonization of sewage sludge and banana stalk : fuel properties of hydrochar and environmental risks of heavy metals. J Environ Chem Eng 2021;9:106051. https://doi.org/10.1016/j.jece.2021.106051.
[5] Zhang C, Ma X, Zheng C, Huang T, Lu X, Tian Y. Co-Hydrothermal carbonization of water hyacinth and sewage sludge: effects of aqueous phase recirculation on the characteristics of hydrochar. Energy Fuel 2020;34:14147–58. https://doi.org/10.1021/acs.energyfuels.0c01991.
[6] Wang Z, Huang J, Wang B, Hu W, Xie D, Liu S, et al. Co-hydrothermal carbonization of sewage sludge and model compounds of food waste: influence of mutual interaction on nitrogen transformation. Sci Total Environ 2021:150997. https://doi.org/10.1016/j.scitotenv.2021.150997.
[7] Wang R, Lin K, Ren D, Peng P, Zhao Z, Yin Q, et al. Energy conversion performance in co-hydrothermal carbonization of sewage sludge and pinewood sawdust coupling with anaerobic digestion of the produced wastewater. Sci Total Environ 2022;803:149964. https://doi.org/10.1016/j.scitotenv.2021.149964.
[8] Poomsawat S, Poomsawat W. Analysis of hydrochar fuel characterization and combustion behavior derived from aquatic biomass via hydrothermal carbonization process. Case Stud Therm Eng 2021;27:101255. https://doi.org/10.1016/j.csite.2021.101255.
[9] Assis EINC, Chirwa EMN. Fuel properties and combustion performance of hydrochars prepared by hydrothermal carbonization of different recycling paper mill wastes. Can J Chem Eng 2022:1. https://doi.org/10.1002/cjce.24708. –15.
[10] Mannarino G, Sarrion A, Diaz E, Gori R, De MA, Mohedano AF. Improved energy recovery from food waste through hydrothermal carbonization and anaerobic digestion. Waste Manag 2022;142:9–18. https://doi.org/10.1016/j.wasman.2022.02.003.
[11] Huddleston SH, Brown GG. Chapter 7: machine learning. INFORMS Anal. Body Knowl.; 2021. p. 231–74. https://doi.org/10.1287/abok.2021.07.
[12] Vieira S, Lopez Pinaya WH, Mechelli A. Introduction to machine learning. Elsevier Inc.; 2019. https://doi.org/10.1016/B978-0-12-815739-8.00001-8.
[13] Bhardwaj P, Tiwari P, Olejar K, Parr W, Kulasiri D. A machine learning application in wine quality prediction. Mach Learn with Appl 2022;8:100261. https://doi.org/10.1016/j.mlwa.2022.100261.
[14] Yin J, Li N. Ensemble learning models with a Bayesian optimization algorithm for mineral prospectivity mapping. Ore Geol Rev 2022;145:104916. https://doi.org/10.1016/j.oregeorev.2022.104916.
[15] Katongtung T, Onsree T, Tippayawong N. Machine learning prediction of biocrude yields and higher heating values from hydrothermal liquefaction of wet biomass and wastes. Bioresour Technol 2022;344:126278. https://doi.org/10.1016/j.biortech.2021.126278.
[16] Cheng F, Belden ER, Li W, Shahabuddin M, Paffenroth RC, Timko MT. Accuracy of predictions made by machine learned models for biocrude yields obtained from hydrothermal liquefaction of organic wastes. Chem Eng J 2022;442:136013. https://doi.org/10.1016/j.cej.2022.136013.
[17] Djandja OS, Salami AA, Wang Z, Duo J, Yin L, Duan P. Random forest-based modeling for insights on phosphorus content in hydrochar produced from hydrothermal carbonization of sewage sludge. Energy 2022;245:123295. https://doi.org/10.1016/j.energy.2022.123295.
[18] Li J, Zhang W, Liu T, Yang L, Li H, Peng H, et al. Machine learning aided bio-oil production with high energy recovery and low nitrogen content from hydrothermal liquefaction of biomass with experiment verification. Chem Eng J 2021;425: 130649. https://doi.org/10.1016/j.cej.2021.130649.
[19] Wang R, Lei H, Liu S, Ye X, Jia J, Zhao Z. The redistribution and migration mechanism of nitrogen in the hydrothermal co-carbonization process of sewage sludge and lignocellulosic wastes. Sci Total Environ 2021;776:145922. https://doi.org/10.1016/j.scitotenv.2021.145922.
[20] Lu X, Ma X, Chen X. Co-hydrothermal carbonization of sewage sludge and lignocellulosic biomass : fuel properties and heavy metal transformation behaviour of hydrochars. Energy 2021;221:119896. https://doi.org/10.1016/j.energy.2021.119896.
[21] Wang R, Lin K, Peng P, Lin Z, Zhao Z, Yin Q, et al. Energy yield optimization of co-hydrothermal carbonization of sewage sludge and pinewood sawdust coupled with anaerobic digestion of the wastewater byproduct. Fuel 2022;326:125025. https://doi.org/10.1016/j.fuel.2022.125025.
[22] Wilk M, Sliz M, Lubieniecki B. Hydrothermal co-carbonization of sewage sludge and fuel additives : combustion performance of hydrochar. Renew Energy 2021; 178:1046–56. https://doi.org/10.1016/j.renene.2021.06.101.
[23] Arachchige G, Kavindi G, Lei Z, Yuan T, Shimizu K. Use of hydrochar from hydrothermal co - carbonization of rice straw and sewage sludge for Cr (VI) bioremediation in soil. Bioresour Technol Reports 2022;18:101052. https://doi.org/10.1016/j.biteb.2022.101052.
[24] Ma J, Luo H, Li Y, Liu Z, Li D, Gai C, et al. Bioresource Technology Pyrolysis kinetics and thermodynamic parameters of the hydrochars derived from co-hydrothermal carbonization of sawdust and sewage sludge using thermogravimetric analysis. 282:133–141, https://doi.org/10.1016/j.biortech.2019.03.007; 2019.
[25] Zhang X, Zhang L, Li A. Hydrothermal co-carbonization of sewage sludge and pinewood sawdust for nutrient-rich hydrochar production : synergistic effects and products characterization. J Environ Manag 2017;201:52–62. https://doi.org/10.1016/j.jenvman.2017.06.018.
[26] Ma J, Chen M, Yang T, Liu Z, Jiao W. Gasification performance of the hydrochar derived from co-hydrothermal carbonization of sewage sludge and sawdust. Energy 2019;173:732–9. https://doi.org/10.1016/j.energy.2019.02.103.
[27] Jia J, Chen H, Wang R, Liu H, Zhao Z, Lei H. Mass and energy equilibrium analysis on co-hydrothermal carbonization coupled with a combined flash-Organic Rankine Cycle system for low-energy upgrading organic wastes. Energy Convers Manag 2021;229:113750. https://doi.org/10.1016/j.enconman.2020.113750.
[28] Lu X, Ma X, Qin Z, Ke C, Chen L, Chen X. Co-hydrothermal carbonization of sewage sludge with wood chip : fuel properties and heavy metal transformation behavior of hydrochars. 2021. https://doi.org/10.1021/acs.energyfuels.1c02145.
[29] Parmar KR, Brown AE, Hammerton JM, Camargo-valero MA, Fletcher LA, Ross AB. Co-processing lignocellulosic biomass and sewage digestate by hydrothermal carbonisation: influence of blending on product. Quality 2022;15:1418.
[30] Weihrich S, Xing X, Zhang X. Co - pyrolysis and HTC refined biomass - biosolid - mixes : combustion performance and residues. Int J Energy Environ Eng 2022;13: 657–69. https://doi.org/10.1007/s40095-021-00453-6.
[31] Wang J, Liu H, Deng H, Jin M, Xiao H, Yao H. Deep dewatering of sewage sludge and simultaneous preparation of derived fuel via carbonaceous skeleton-aided thermal hydrolysis. Chem Eng J 2020;402:126255. https://doi.org/10.1016/j.cej.2020.126255.
[32] Ebrahimi M, Hassanpour M, Rowlings DW, Bai Z, Dunn K, Hara IMO, et al. Effects of lignocellulosic biomass type on nutrient recovery and heavy metal removal from digested sludge by hydrothermal treatment. J Environ Manag 2022;318:115524. https://doi.org/10.1016/j.jenvman.2022.115524.
[33] Zhang S, Pi M, Su Y, Xu D, Xiong Y, Zhang H. Biomass and Bioenergy Physiochemical properties and pyrolysis behavior evaluations of hydrochar from co-hydrothermal treatment of rice straw and sewage sludge. Biomass Bioenergy 2020;140:105664. https://doi.org/10.1016/j.biombioe.2020.105664.
[34] Peng C, Zhai Y, Zhu Y, Wang T, Xu B. Investigation of the structure and reaction pathway of char obtained from sewage sludge with biomass wastes , using hydrothermal treatment. J Clean Prod 2017;166:114–23. https://doi.org/10.1016/j.jclepro.2017.07.108.
[35] Wang W, Chen W, Jang M. Characterization of hydrochar produced by hydrothermal carbonization of organic sludge. Futur Cities Environ 2020;6:1–10. https://doi.org/10.5334/fce.102.
[36] Chen T, Guestrin C. XGBoost: a scalable tree boosting system. Proc ACM SIGKDD Int Conf Knowl Discov Data Min 2016;13–17. https://doi.org/10.1145/2939672.2939785. Augu:785–94.
[37] Leng L, Zhang W, Chen Q, Zhou J, Peng H, Zhan H, et al. Machine learning prediction of nitrogen heterocycles in bio-oil produced from hydrothermal liquefaction of biomass. Bioresour Technol 2022;362:127791. https://doi.org/10.1016/j.biortech.2022.127791.
[38] Friedman JH. Greedy function approximation: a gradient boosting machine. Ann Stat 2001;29:1189–232. https://doi.org/10.1214/aos/1013203451.
[39] Djandja S, Wang Z, Wang F, Xu Y, Duan P. Pyrolysis of municipal sewage sludge for biofuel production : a review. 2020. https://doi.org/10.1021/acs.iecr.0c01546.
[40] Hameed Z, Naqvi SR, Naqvi M, Ali I, Taqvi SAA, Gao N, et al. A comprehensive review on thermal coconversion of biomass, sludge, coal, and their blends using thermogravimetric analysis. J Chem 2020;2020. https://doi.org/10.1155/2020/5024369.
[41] Rorat A, Courtois P, Vandenbulcke F, Lemiere S. Sanitary and environmental aspects of sewage sludge management. In: Ind. Munic. Sludge emerg. Concerns scope resour. Recover. Elsevier Inc.; 2020. p. 155–80. https://doi.org/10.1016/B978-0-12-815907-1.00008-8.
[42] Hamood A, Khatib JM. Sustainability of sewage sludge in construction. second ed. Elsevier Ltd.; 2016. https://doi.org/10.1016/b978-0-08-100370-1.00024-x.
[43] Van Berg JJD. Effects of sewage sludge disposal. Land Degrad Dev 1993;4:407–13. https://doi.org/10.1002/ldr.3400040426.
[44] Gao N, Kamran K, Quan C, Williams PT. Thermochemical conversion of sewage sludge: a critical review. Prog Energy Combust Sci 2020;79:100843. https://doi.org/10.1016/j.pecs.2020.100843.
[45] Yan M, Liu Y, Song Y, Xu A, Zhu G, Jiang J. Comprehensive experimental study on energy conversion of household kitchen waste via integrated hydrothermal carbonization and supercritical water gasi fi cation. Energy 2022;242:123054. https://doi.org/10.1016/j.energy.2021.123054.
[46] Peng C, Zhai Y, Hornung A, Wang B, Li S, Wang T, et al. In-depth comparison of morphology , microstructure , and pathway of char derived from sewage sludge and relevant model compounds. Waste Manag 2020;102:432–40. https://doi.org/10.1016/j.wasman.2019.11.007.
[47] Zhai Y, Peng C, Xu B, Wang T, Li C. Hydrothermal carbonisation of sewage sludge for char production with different waste biomass : effects of reaction temperature and energy recycling. Energy 2017;127:167–74. https://doi.org/10.1016/j.energy.2017.03.116.
[48] Phillips CL, Meyer KM, Garcia-Jaramillo M, Weidman CS, Stewart CE, Wanzek T, et al. Towards predicting biochar impacts on plant-available soil nitrogen content. Biochar 2022;4:1–15. https://doi.org/10.1007/s42773-022-00137-2.
[49] He M, Zhu X, Dutta S, Khanal SK, Lee KT, Masek O, et al. Catalytic co-hydrothermal carbonization of food waste digestate and yard waste for energy application and nutrient recovery. Bioresour Technol 2022;344:126395. https://doi.org/10.1016/j.biortech.2021.126395.
[50] Zhang C, Dong H, Geng Y, Liang H, Liu X. Machine learning based prediction for China's municipal solid waste under the shared socioeconomic pathways. J Environ Manag 2022;312:114918. https://doi.org/10.1016/j.jenvman.2022.114918.
[51] Borbolla-gaxiola JE, Ross AB, Dupont V. Multi-variate and multi-response analysis of hydrothermal carbonization of food waste: hydrochar composition and solid fuel characteristics. Energies 2022;15. https://doi.org/10.3390/en15155342.

[52] Kang S, Li X, Fan J, Chang J. Characterization of hydrochars produced by hydrothermal carbonization of lignin, cellulose, d-xylose, and wood meal. Ind Eng Chem Res 2012;51:9023–31. https://doi.org/10.1021/ie300565d.
[53] Ameen M, Zamri NM, May ST, Azizan MT, Aqsha A. Effect of acid catalysts on hydrothermal carbonization of Malaysian oil palm residues (leaves. fronds , and shells) for hydrochar production 2022:103–14.
[54] Zhang C, Ma X, Chen X, Tian Y, Zhou Y, Lu X, et al. Conversion of water hyacinth to value-added fuel via hydrothermal carbonization. Energy 2020;197:117193. https://doi.org/10.1016/j.energy.2020.117193.
[55] Aliyu M, Iwabuchi K, Itoh T. Improvement of the fuel properties of dairy manure by increasing the biomass-to-water ratio in hydrothermal carbonization. PLoS One 2022;17:1–16. https://doi.org/10.1371/journal.pone.0269935.